An acetylation-mediated chromatin switch governs H3K4 methylation read-write capability

Kanishk Jain[1,2], Matthew R. Marunde[3], Jonathan M. Burg[3], Susan L. Gloor[3], Faith M. Joseph[4], Zachary B. Gillespie[3], Keli L. Rodriguez[3], Sarah A. Howard[3], Irina K. Popova[3], Nathan W. Hall[3], Anup Vaidya[3], Spencer W. Cooke[1], Kevin E. W. Namitz[5], Bethany C. Taylor[4], Ellen N. Weinzapfel[3], Marcus A. Cheek[3], Matthew J. Meiners[3], Krzysztof Krajewski[1,2], Michael S. Cosgrove[6], Nicolas L. Young[4], Michael-Christopher Keogh[3*], and Brian D. Strahl[1,2,7*]

[1]Department of Biochemistry and Biophysics, University of North Carolina at Chapel Hill, School of Medicine, Chapel Hill, NC;
[2]Lineberger Comprehensive Cancer Center, University of North Carolina at Chapel Hill, School of Medicine, Chapel Hill, NC;
[3]EpiCypher, Inc., Durham, NC;
[4]Verna & Marrs McLean Department of Biochemistry and Molecular Biology, Baylor College of Medicine, Houston, TX;
[5]Pennsylvania State University, State College, PA;
[6]Department of Biochemistry and Molecular Biology, Upstate Medical University, Syracuse, NY
[7]Lead Contact
*Correspondence: mkeogh@epicypher.com and brian_strahl@med.unc.edu

ABSTRACT

In nucleosomes, histone N-terminal tails exist in dynamic equilibrium between free/accessible and collapsed/DNA-bound states. The DNA-bound state is expected to impact histone N-termini availability to the epigenetic machinery. Notably, H3 tail acetylation (K9ac, K14ac, K18ac) is linked to increased engagement of H3K4me3 by the BPTF PHD finger, but it is unknown if this mechanism has broader extension. Here we show that *cis* H3 tail acetylation promotes nucleosomal accessibility to other H3K4 methyl readers, and further extends to H3K4 writers, notably methyltransferase MLL1. This regulation is nucleosome-dependent and also observed *in vivo*, where H3 acetylation correlates with increased levels of *cis* H3K4me. These observations reveal an acetylation 'chromatin switch' on the H3 N-terminal tail that modulates the accessibility and function of H3K4 methylation in chromatin. Our findings also resolve the long-standing question of why H3K4me3 levels are linked with H3 acetylation.

INTRODUCTION

In the epigenetic landscape, histone proteins are often variably chemically modified by "writer" enzymes (Jenuwein and Allis, 2001; Strahl and Allis, 2000). The writer-installed post-translational modifications (PTMs) are recognized by "reader" proteins and removed by "eraser" enzymes. This interplay of PTMs comprises the "histone code," and it has a central function in regulating chromatin organization and activity. For example, methylated/acylated lysine or methylated arginine residues of histones can recruit transcription factors to activate or repress transcription (Strahl and Allis, 2000; Su and Denu, 2016); mitotically phosphorylated serine/threonine residues can regulate reader binding established at earlier stages of the cell cycle (Rossetto et al., 2012); or ubiquitinated lysine can impact the maintenance of DNA methylation (Vaughan et al., 2021). As the complex language of histone PTMs is being dissected, it has become clear that multivalent interactions with reader proteins can influence chromatin structure and DNA accessibility, thereby regulating gene transcription and other DNA-templated events (Su and Denu, 2016; Taylor and

48 Young, 2021; Young et al., 2010). In this manner, combinatorial PTMs can more effectively
49 engage different chromatin-binding modules, promoting distinct outcomes versus either PTM
50 alone.

51 The bulk of chromatin PTM research has used peptides, even though histones exist *in*
52 *vivo* in a heteromeric complex with DNA (i.e., the nucleosome). It is becoming increasingly clear
53 that studying histone PTM engagement in the nucleosome context provides a more accurate
54 understanding of the histone code. Particularly, the highly charged histone tails interact directly
55 with nucleosomal DNA, restricting access for PTM recognition by reader proteins (Ghoneim et al.,
56 2021; Marunde et al., 2022a; Morrison et al., 2018)**.** Studies with BPTF PHD suggest acetylation
57 releases the H3 N-terminal tail from the nucleosome surface, such that H3K4me3 becomes more
58 readily engaged by the PHD finger (Marunde et al., 2022a; Morrison et al., 2018)**.**

59 Considerable research effort has focused on dissecting the direct (and multivalent)
60 engagement of chromatin via histone PTM-reader protein interactions. However, less appreciated
61 are any indirect effects of PTMs on histone tail accessibility/nucleosome dynamics (*e.g.,* via
62 charge neutralization). In this report, we demonstrate enhanced nucleosome binding by a range
63 of H3K4 readers when the histone tail is concomitantly acetylated (one or more of K9ac, K14ac,
64 and K18ac). Furthermore, from *in vitro* enzymatic assays, we found that neighboring acetylation
65 of the H3 tail was a prerequisite switch that enabled MLL1 complex (MLL1C) (Rao and Dou, 2015)
66 to robustly methylate H3K4. Interestingly, mass spectrometric proteomic analyses of mammalian
67 cells in a timed response to sodium butyrate (a broad-spectrum lysine deacetylase (KDAC)
68 inhibitor) revealed a tight correlation of H3K4 methylation with *cis* acetylation. Our findings define
69 a critical aspect of chromatin regulation: *i.e.,* crosstalk by histone tail accessibility. The findings
70 also provide a molecular basis for the long-standing connection between H3K4 methylation and
71 H3 acetylation (Garcia et al., 2007; Taverna et al., 2007), and resolve the directionality of these
72 correlations: *cis* hyperacetylation of the H3 tail precedes, and is largely a prerequisite for, H3K4

73 methylation. Thus, the establishment of sites of H3K4me3 and activation of transcription occur by
74 a sequence of modifications of the same histone molecule.
75
76 **RESULTS**
77 **PHD finger readers show narrowed selectivity for histone tail PTMs on mononucleosomes**
78 **versus peptides**
79 How histone readers engage nucleosomes is an extensively researched area of chromatin
80 biology. Most investigators have used PTM-defined histone peptides to characterize reader
81 binding, although these often display a refined preference to similarly modified nucleosomes
82 (Marunde et al., 2022a, 2022b; Morgan et al., 2021; Morrison et al., 2018)**.** To further assess this
83 potential, we used the dCypher® approach (Jain et al., 2020; Marunde et al., 2022b; Morgan et
84 al., 2021; Weinberg et al., 2021) to measure the interactions of three PHD readers (from KDM7A,
85 DIDO1, and MLL5: the queries) with PTM-defined peptides and nucleosomes (the potential
86 targets). As expected (Jain et al., 2020), each GST-PHD fusion showed a preference for H3K4-
87 methylated peptides and, particularly, to higher methyl states (*i.e.*, KDM7A bound me2/me3,
88 DIDO1 bound me1/me2/me3, and MLL1 bound me1/me2/me3; **Figure 1A**). We further observed
89 no impact of co-incident acetylation on H3K4me3 binding in the peptide context (compare
90 H3K4me3 to H3K4me3K9acK14acK18ac [hereafter H3K4me3tri^{ac}]). However on nucleosomes
91 each GST-PHD showed reduced and restricted binding to H3K4me3 over the lower methyl states,
92 and this interaction was dramatically enhanced (~10-15-fold) by co-incident acetylation (as at
93 H3K4me3tri^{ac}; **Figure 1B**). The notable impact of acetylation state on binding of these readers in
94 the nucleosome context (also recently observed for the BPTF PHD domain (Marunde et al.,
95 2022a; Morrison et al., 2018)) led us to consider additional implications of this interplay.
96 Histone tail lysine acetylation (Kac) can directly recruit residue-specific readers, *e.g.,*
97 bromodomains (Musselman et al., 2012), but acetylation also neutralizes the positive charge on
98 lysine residues and relieves their interaction with negatively charged DNA (*i.e.*, altering the

99 histone tail-DNA binding equilibrium) (Marunde et al., 2022a; Morrison et al., 2018). In the
100 nucleosome context, this decreased histone-DNA binding supports the increased engagement of
101 reader domains that have no direct affinity for the Kac. Conversely, isolated histone tail peptides
102 are 'constitutively open' (no DNA to engage), and thus not subject to this mode of regulation. We
103 surmised that the effect of charge neutralization to increase H3K4me3 accessibility could have
104 application beyond reader domains, perhaps also applying to enzymes that target H3K4.
105

106 **H3 N-terminal acetylation significantly enhances MLL1C methylation of nucleosomal H3K4**

107 To investigate if acetylation makes the H3 N-terminus more accessible for modification, we
108 performed enzymatic assays with the MLL1 core complex (MLL1C) responsible for H3K4me3
109 (Rao and Dou, 2015; Sha et al., 2020) and nucleosome substrates ± accompanying
110 polyacetylation (H3K9acK14acK18ac; hereafter H3tri^{ac}) (see **Methods**). In an endpoint assay at
111 constant enzyme and substrate concentrations (and [*methyl*-^{3}H]-SAM donor), we observed a
112 significant increase in net methylation when the H3 tail was also acetylated (**Figure 2A**). As
113 expected, methylation by MLL1C sequentially decreased towards H3K4 mono-, di-, and
114 trimethylated nucleosomal substrates, being undetectable on H3K4me3 (which also confirmed
115 MLL1C targeting of this specific residue). Despite this, methyl group incorporation to each H3K4
116 methyl state substrate was consistently enhanced by accompanying H3tri^{ac} (**Figure 2A**). Of note,
117 we further tested the viability of synthetic methyllysine analogs (MLAs) (Simon and Shokat, 2012)
118 ± H3tri^{ac} as MLL1C substrates and observed no activity, indicating the unsuitability of MLAs for
119 such studies (**Figure S2D**).

120 We also measured the steady-state kinetics of MLL1C methylation of nucleosomes with
121 each H3K4 methyl state ± H3tri^{ac}, and again observed that acetylation increased
122 methyltransferase activity (**Figure 2B**). Using an extra sum-of-squares F-test, methylation data
123 for the H3tri^{ac} nucleosomes were indicative of positive cooperativity because of better fit (p =
124 0.0216) to the Hill equation (Weiss, 1997) (**Figure 2B** v. **Figure S2C**; **Table 1** v. **Table S1**).

125 Because of the low level of enzymatic activity towards the unacetylated nucleosomes we could
126 not make a statistically significant comparison between the Hill and Michaelis-Menten fits. There
127 have been limited studies of MLL1C activity on nucleosomes (Park et al., 2019; Patel et al., 2011;
128 Xue et al., 2019), so an overlooked potential allostery is understandable given the complex
129 possible interactions between this enzyme and substrate (Lee et al., 2021; Park et al., 2019)

130 Interestingly, although overall k_{cat} was ~17-fold greater for the H3tri^{ac} nucleosomes, the
131 $K_{0.5}$ values (substrate concentration at half-maximal velocity/half-saturation for an allosterically
132 regulated enzyme) were indistinguishable (**Table 1**). Therefore, although MLL1C catalytic
133 efficiency toward H3tri^{ac} nucleosomes was enhanced by an increase in k_{cat}, this catalytic efficiency
134 was not driven by $K_{0.5}$, which suggested no increase in relative binding affinity. To further examine
135 this, we used dCypher to examine potential binding between MLL1C query and a selection of
136 nucleosome targets: unmodified, H3N∆32 (lacking the first 32 residues of H3), Tailless (trypsin-
137 digested nucleosomes to remove N- and C-terminal histone tails), and H3tri^{ac}. At 50 mM NaCl,
138 we observed no compelling difference in MLL1C binding between any of these nucleosomes
139 (**Figure 2C**). This finding agreed with structural studies where binding between MLL1C and the
140 nucleosome occurs primarily through interactions with nucleosomal DNA and, to a lesser degree,
141 the H4 N-terminal tail (Lee et al., 2021; Park et al., 2019). Thus, the increased H3K4 methylation
142 observed when the H3 N-terminal tail was acetylated was not due to enhanced MLL1C –
143 nucleosome binding. Instead, H3 acetylation likely released the histone tail from the nucleosome,
144 thereby increasing the apparent H3K4 concentration and enhancing methylation (**Figure 2D**).
145

146 **Cellular level of H3K4 methylation is coupled to H3 N-terminal tail hyperacetylation**

147 The above data suggested a molecular model for how the H3 N-terminal tail, via *cis* acetylation,
148 becomes available for H3K4 reader binding or enzymatic modification *in vitro*. To determine if
149 such acetylation could function as an accessibility switch *in vivo*, we used middle-down mass
150 spectrometry on acid-extracted histones from asynchronous MCF-7 breast cancer cells to

151 measure the relationship between H3K4 methylation and tail acetylation on the same H3
152 proteoforms (Holt et al., 2021; Smith and Kelleher, 2013). As expected (Garcia et al., 2007; Peach
153 et al., 2012; Young et al., 2009), the absolute amounts of H3K4me3 and higher Kac states (3ac,
154 4ac, and 5ac) across adjacent lysine residues were extremely low (**Figure S3A**). Nonetheless,
155 H3K4me3 (<1% of total H3) was strictly associated with molecules that contained multiple
156 acetylations (also <1% of total H3; **Figure 3A**). Given this relationship, we next addressed the
157 hypothesis that increased lysine acetylation may release the H3 tail for more effective H3K4
158 methylation (*i.e.*, acetylation precedes methylation). We treated MCF-7 cells with the KDAC
159 inhibitor sodium butyrate and collected samples at multiple timepoints to measure the levels of
160 H3K4methylation with *cis* acetylation. H3 poly-acetylation rapidly increased upon butyrate
161 treatment (**Figure S3B** and **Table S2**), as would be predicted (Holt et al., 2019; Young et al.,
162 2009). While H3K4me3 levels most dramatically increased in tandem with the 5ac H3 proteoform
163 (**Figure 3B**), we observed an associated increase in all H3K4 methyl states as the H3 tail was
164 increasingly acetylated (**Figures 3C** and **S3C; Table S2**). These findings support a direct link
165 whereby acetylation releases nucleosome-bound H3 tails to available H3K4 methyltransferases
166 for subsequent methylation (see model in **Figure 2D**). Such a chromatin-switch may also help
167 cells to translate short-term acetylation signals at gene promoters to longer-term heritable marks
168 of epigenetic memory (Greer et al., 2014; Hörmanseder et al., 2017; Muramoto et al., 2010; Ng
169 et al., 2003).
170

171 **DISCUSSION**

172 While previous investigations identified a link between H3K4 methylation and H3 acetylation in
173 diverse species (Garcia et al., 2007; Strahl et al., 1999; Taverna et al., 2007; Young et al., 2009),
174 the molecular basis for this link was unknown, and we posit the H3 acetyl 'chromatin switch' is
175 conserved across eukaryotes. Our new understanding of the dynamic structure of nucleosome
176 histone tails, alternating between collapsed *(i.e.*, nucleosome-bound) and accessible forms

177 (Marunde et al., 2022a; Morrison et al., 2018), has made more plausible the notion that tail
178 availability could be driven by combinatorial *cis* acetylation to directly promote H3K4 methylation.
179 In this study, we showed that hyperacetylation of the H3 N-terminal tail promoted rapid
180 accumulation of H3K4 methylation in *cis*, most likely by increasing availability of the substrate
181 residue to the MLL1C active site. This finding was supported by our *in vitro* enzymatic and *in vivo*
182 mass spectrometric analyses. Methylation assays with MLL1C revealed significantly enhanced
183 enzyme activity towards nucleosome substrates with co-incident acetylated (H3tri^{ac}) over
184 unmodified H3 (**Figure 2A-B; Table 1**). dCypher assays demonstrated that the acetylation-
185 mediated increase in H3K4 methylation does not involve stabilized interactions between MLL1C
186 and the nucleosome (**Figure 2C**). In agreement with these *in vitro* findings, middle-down mass
187 spectrometry showed that H3 hyperacetylation and H3K4 methylation co-occurred on the same
188 histone tails in actively cycling cells; furthermore, upon butyrate treatment H3K4 methylation
189 increased for the most highly acetylated proteoforms (**Figures 3** & **S3**). The *in vivo* relationship
190 required higher degrees of acetylation (preferring at least four acetyl groups per molecule: *e.g.*,
191 H3K9acK14acK18acK23acK27ac) for most effective conversion to the H3K4me3 state. Together
192 with binding studies that identify the positive impact of *cis* H3 tail hyperacetylation on H3K4 reader
193 engagement (**Figures 1** & **S1**) (Marunde et al., 2022a; Morrison et al., 2018), our findings suggest
194 a molecular switch that governs when and where the histone H3 N-terminus is available for H3K4-
195 related transactions. Such a switch could be used to establish and heritably maintain the location
196 and function of transcriptional promoters across the genome.

197 A continued observation from this study is that the binding preference of readers (in this
198 case PHD-fingers that engage histone H3K4) are narrowed on nucleosomes relative to histone
199 peptides (**Figure 1** & **S1**) (Marunde et al., 2022a; Morgan et al., 2021). This difference in binding
200 further highlights the importance of using nucleosomes as physiologically relevant substrates for
201 *in vitro* interaction assays. We also add to the literature confirming importance of the physiological
202 substrate for enzymatic studies (Strelow et al., 2016; Stützer et al., 2016). In this regard our

203 steady-state kinetic methylation assays with MLL1C revealed an intriguing (and previously
204 undescribed) positive cooperativity with its preferred nucleosome substrates (**Figure 2B** versus
205 **S2C**). It is important to consider the suggestion that allosteric factors could regulate interactions
206 between MLL1C and the nucleosome, especially since previous kinetic analyses of this
207 [enzyme:substrate] pair did not address such behavior (Park et al., 2019; Xue et al., 2019).
208 However, positive cooperativity was not evident at the level of MLL1C - nucleosome binding,
209 which was independent of substrate identity (*i.e.*, ± H3tri^{ac}) at ionic conditions similar to the
210 catalytic assay (**Figure 2C**). Still to be determined are the signals that drive and regulate this
211 cooperativity and its function in MLL1-catalyzed methylation, especially in a higher-order
212 chromatin context.

213 Our study highlights a previously unrecognized regulatory mechanism for how writers
214 might engage the histone H3 tail (specifically at H3K4) *in vivo*. Although this work focused on H3,
215 it will be important to ascertain the consequence of acetylation (or indeed other acylation)-
216 mediated changes in accessibility and the function of modifiers and readers of the other core
217 histones (H2A, H2B, and H4). A more detailed analysis of how to regulate histone tail accessibility
218 (in *cis* and *trans*) will likely add to the already complex language of the histone code.

219 Epigenetic studies have identified H3K4 methylation and H3 acetylation as active marks
220 because of their co-occupancy on promoters and gene bodies of transcribed genes (Santos-Rosa
221 et al., 2002; Strahl et al., 1999; Wozniak and Strahl, 2014). Our findings agree with these
222 observations regarding H3K4 methylation, but it will be interesting to determine whether PTMs
223 such as H3K9 methylation, normally (but not exclusively (Barral et al., 2022; Mauser et al., 2017))
224 a repressive mark, show similarly enhanced histone accessibility due to *cis* acetylation.

225 **ACKNOWLEDGEMENTS**

226 KJ is supported by a Postdoctoral Training Fellowship from the National Institutes of Health (NIH;
227 T32CA217824) to the UNC Lineberger Cancer Center and a Postdoctoral Fellowship from the
228 American Cancer Society (PF-20-149-01-DMC). This work was also supported by NIH grants to
229 NLY (R01GM139295, P01AG066606, and R01CA193235), MSC (R01CA140522), to EpiCypher
230 (R44GM117683, R44CA214076 and R44GM116584), and to BDS (R35GM126900). We thank
231 colleagues for the generous supply of materials (see **Methods**) and members of the Cosgrove,
232 Young, *EpiCypher* and Strahl labs for helpful discussions and suggestions.

233

234 **AUTHOR CONTRIBUTIONS**

235 KJ, MRM, JMB, MCK, and BDS conceptualized and designed the study. ZBG, SAH, MAC, and
236 MJM assembled and validated PTM-defined dNucs and versaNucs. KK synthesized histone
237 peptides used in versaNuc construction. MM, JB, SLG, KLR, IKP, NWH, AV, and ENW performed
238 dCypher assays and analyzed data with input from KJ, MCK, and BDS. KEWN and MSC purified
239 MLL1C for enzymatic analyses. KJ and SWC purified his-tagged MLL1C for binding assays.
240 Methylation assays were performed and analyzed by KJ and SWC. MCF7 cells were cultured by
241 KJ, and mass spectrometry was performed and analyzed by FJ, BCT, and NY. KJ and BDS wrote
242 the first draft of the manuscript and all authors contributed to subsequent editing.

243

244 **DECLARATIONS OF INTEREST**

245 MSC owns stock/serves on the Consultant Advisory Board for Kathera Bioscience Inc. and holds
246 US patents (8,133,690; 8,715,678; and 10,392,423) for compounds/methods for inhibiting
247 SET1/MLL family complexes. EpiCypher is a commercial developer and supplier of reagents (e.g.,
248 PTM-defined semi-synthetic nucleosomes; dNucs™ and versaNucs®) and platforms (*e.g.,*
249 dCypher®) used in this study. MCK and BDS are board members of EpiCypher.

250 **FIGURES AND TABLES**

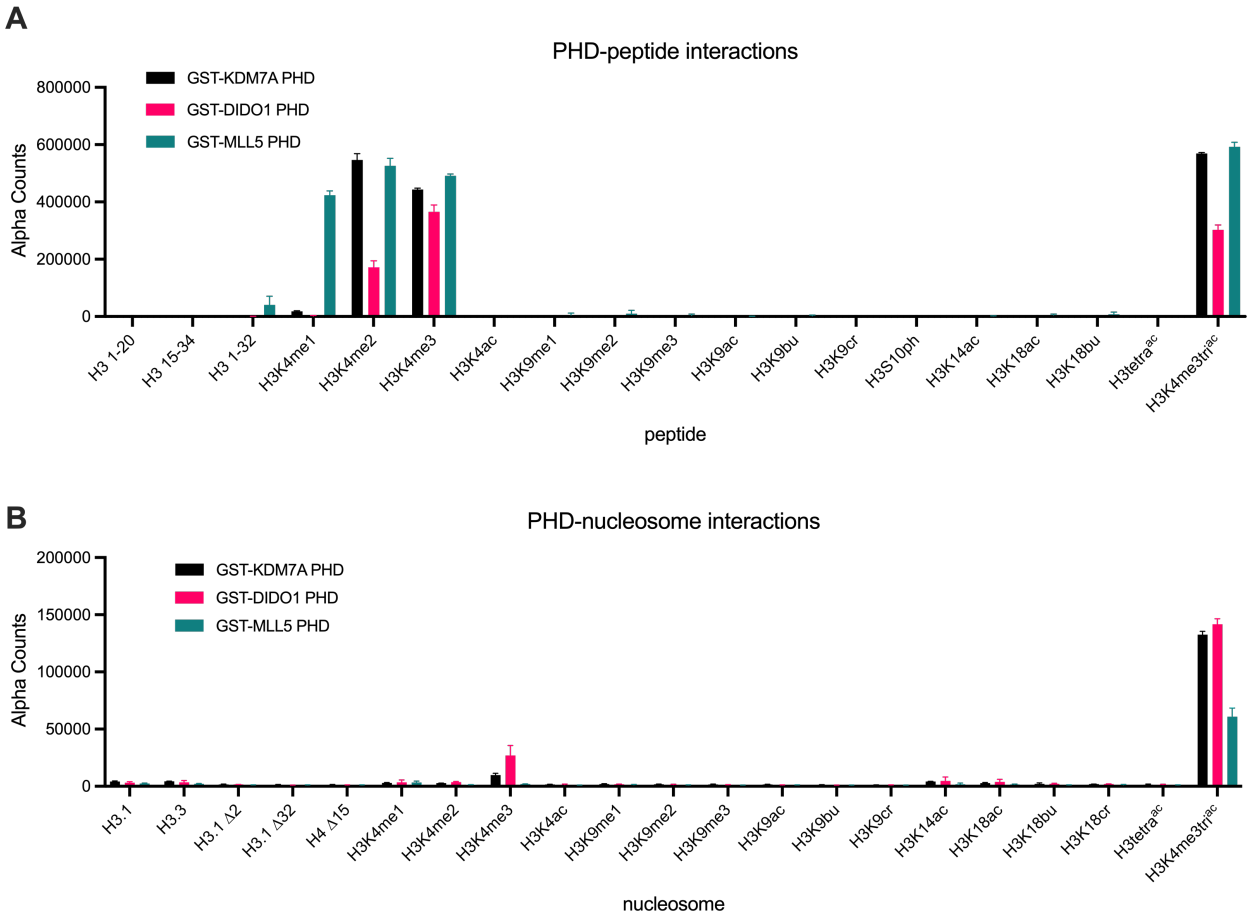

251
252 **Figure 1. PHD finger reader domains show restricted binding on PTM-defined peptides vs.**
253 **nucleosomes.** *dCypher* assay alpha counts for interaction of GST-PHD queries (9.5 nM KDM7A
254 (Uniprot #Q6ZMT4; residues 1-100); 2.4 nM DIDO1 (Uniprot #Q9BTC0; residues 250-340); 18
255 nM MLL5 (Uniprot #Q8IZD2; residues 100-180)) with PTM-defined peptides (**A**) *vs.* nucleosomes
256 (**B**) (the potential targets). All error bars represent the range of two replicates. Key: H3.1N Δ2,
257 H3.1N Δ32 and H4N Δ15 are nucleosomes assembled with histones lacking the indicated N-
258 terminal residues of H3.1 or H4. All data was plotted using GraphPad Prism 9.0.

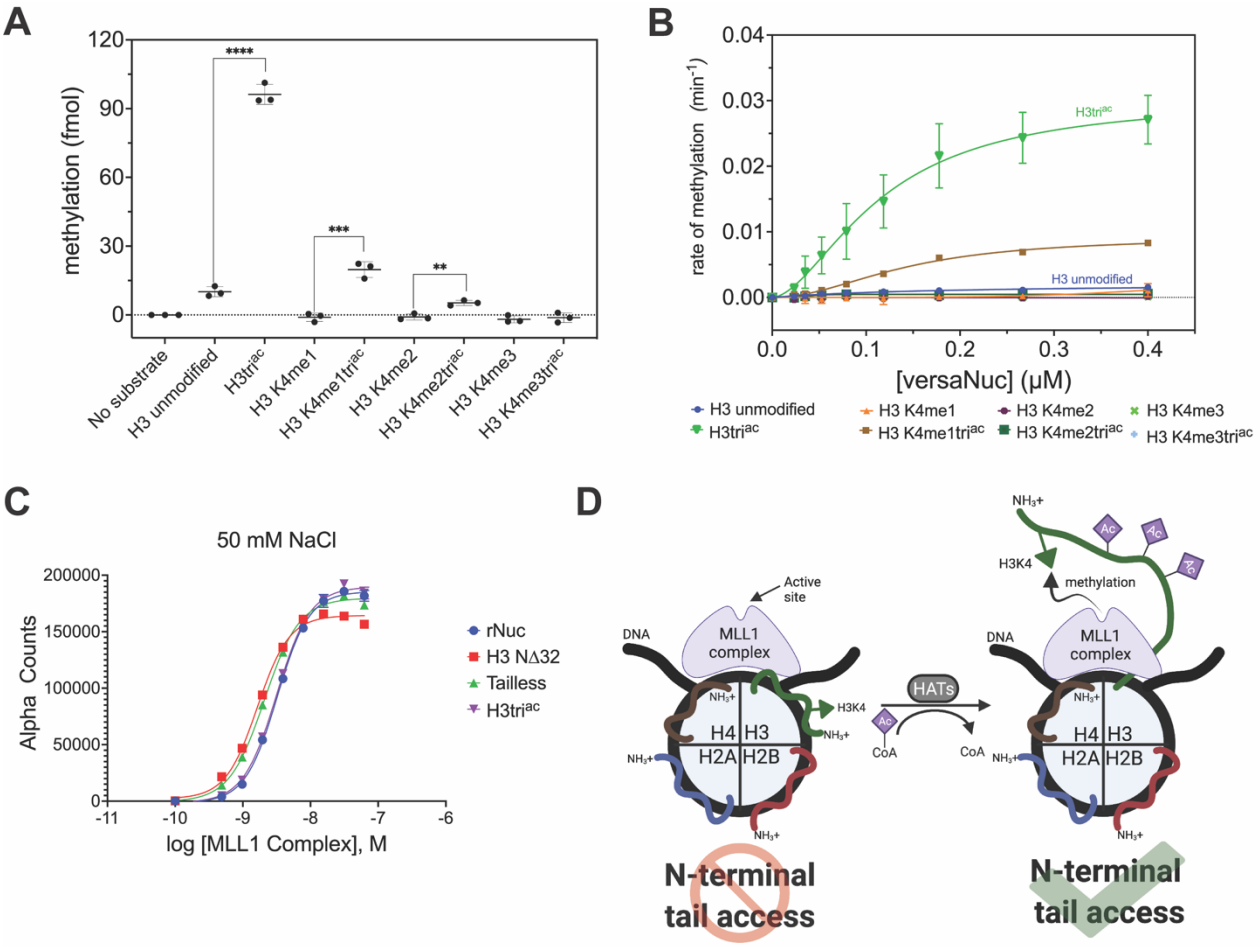

Figure 2. In the nucleosome context MLL1C methylation activity on H3K4 is significantly enhanced by co-incident H3tri^{ac}. A) Endpoint methylation assays of H3K4me0 (unmodified)-me1-me2-me3 nucleosomes and their cognate H3K9ac14ac18ac (H3tri^{ac}) partners (all 100 nM) with MLL1C (4nM). Reactions performed in triplicate with error bars as S.D. *p*-values were determined using a two-tailed t test: **** = <0.0001, *** = 0.0008, ** = 0.0038. **B)** MLL1 complex (4 nM) methylation activity on H3K4me0-me1-me2-me3 nucleosomes and their cognate H3tri^{ac} partners (all substrates: 1.5-fold serial dilution, 0-0.4 μM). Reactions performed in triplicate with error bars as S.D. **C)** dCypher binding curves of 6HIS-tagged MLL1C (concentration as noted) with PTM-defined nucleosomes (20 nM). Error bars represent the range of two replicates. **D)** Graphical model for how H3 N-terminal tail acetylation may regulate H3K4 methylation by MLL1C.

271 Nucleosomal DNA is represented in black; each histone is as labeled, with the core histone N-

272 terminal tails colored to distinguish. MLL1C is in purple.

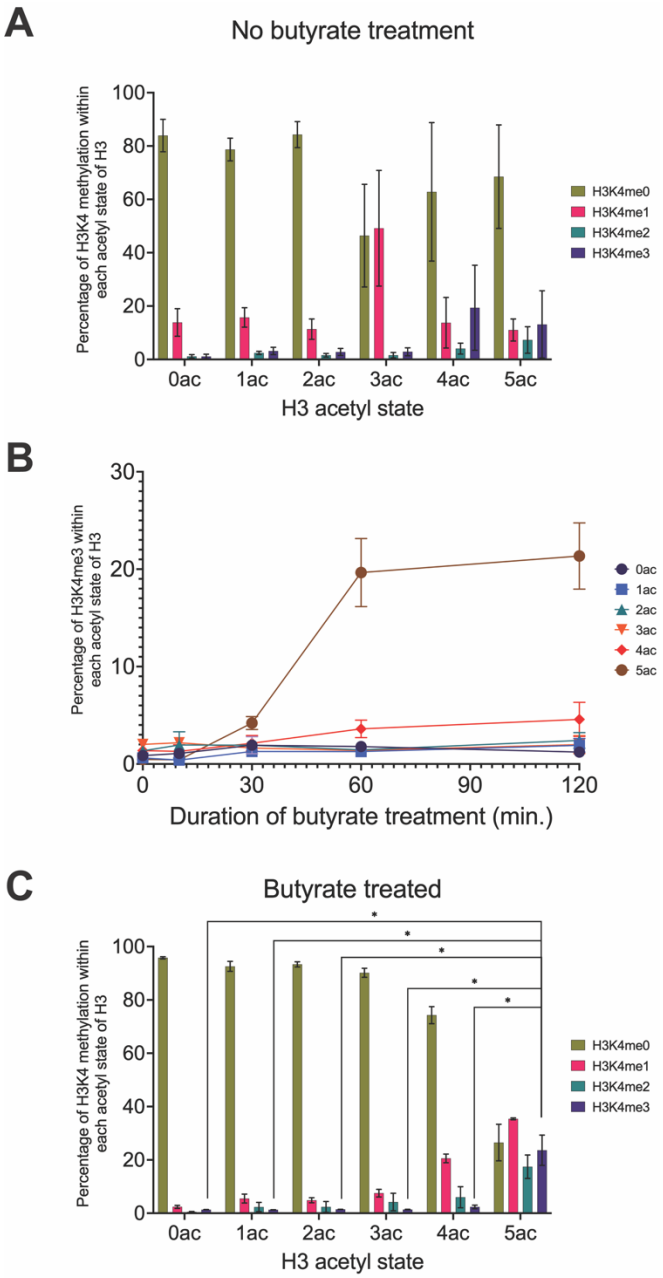

Figure 3. Middle-down MS analysis reveals a hierarchical dependence between H3K4 methylation and *cis* H3 acetylation in MCF-7 cells. A) Occupancy of H3K4 methyl states (me0-1-2-3) within each H3 acetyl state (0ac to 5ac) in asynchronous MCF-7 cells. **B)** Time course of H3K4me3 accumulation with respect to each H3 acetyl state after butyrate treatment. **C)** Occupancy of H3K4 methyl states within each H3 acetyl state after butyrate treatment (60 mins).

280 Asterisks represent *p*-values < 0.05. All data were collected in biological triplicate with error bars

281 representing S.E.M.

282 **TABLE 1:** Steady-state Hill kinetic parameters
283

Substrate	$K_{0.5}$ (μM)	k_{cat} (min^{-1})	h (Hill coefficient)	R^2
H3 unmodified	0.13 ± 0.06	0.0018 ± 0.0004	1.213 ± 0.3430	0.8810
H3 K9/14/18Ac	0.12 ± 0.02	0.0304 ± 0.0036	1.741 ± 0.3528	0.9228
H3 K4me1	n.d.[a]	n.d. [a]	n.d. [a]	0.3186
H3 K4me1 K9/14/18Ac	0.14 ± 0.008	0.0092 ± 0.0004	2.032 ± 0.1333	0.9920
H3 K4me2	n.d. [a]	n.d. [a]	n.d. [a]	-0.1746
H3 K4me2 K9/14/18Ac	0.042 ± 0.005	0.0005 ± 0.00004	5.349 ± 2.682	0.8155
H3 K4me3	n.d. [a]	n.d. [a]	n.d. [a]	n.d. [a]
H3 K4me3 K9/14/18Ac	n.d. [a]	n.d. [a]	n.d. [a]	n.d. [a]

284

285 [a] = methylation signal was indistinguishable from background: kinetic parameters could not be

286 determined.

287 **METHODS**

288 *Expression and purification of GST-tagged PHD reader proteins*

289 Recombinant expression constructs for GST-tagged PHD domains from KDM7A (Uniprot
290 #Q6ZMT4; residues 1-100), DIDO1 (Uniprot #Q9BTC0; residues 250-340), and MLL5 (Uniprot
291 #Q8IZD2; residues 100-180) were synthesized by BioMatik Corporation in a pGEX-4T-1 vector
292 and provided by Dr. Mark T. Bedford (UT MD Anderson Cancer Center). These proteins were
293 expressed and purified as described (Jain et al., 2020).

294

295 *Expression, purification, and assembly of the MLL1 core complex (MLL1C)*

296 Methods for the expression, purification, and assembly of MLL1 core complex (MLL1C) were
297 adapted from published protocols (Usher et al., 2021). A polycistronic recombinant expression
298 construct containing the MLL1 SET domain (Uniprot Q03164; residues 3745-3969), WDR5
299 (Uniprot P61964; residues 2-334), RbBP5 (Uniprot Q15291; residues 1-538) and Ash2L (Uniprot
300 Q9UBL3-3; residues 1-534) (MWRA construct) in pST44 vector was a kind gift from Dr. Song Tan
301 (Tan et al., 2005). WDR5 was cloned with an N-terminal hexahistidine (6HIS) tag and TEV
302 protease site to enable purification via immobilized metal affinity chromatography (IMAC), and
303 enzymatic cleavage for tag removal. Rosetta pLysS *E. coli* cells were transformed with the
304 plasmid and grown on LB plates with 50 μg/mL carbenicillin. Single colonies were used to
305 inoculate 50 mL starter cultures of Terrific Broth (TB) containing 50 μg/mL carbenicillin and grown
306 at 37°C for 16 hours. This culture was transferred to 1L of TB + carbenicillin and grown to OD_{600}
307 ~0.6 (37°C, 200 RPM, ~ 4 hours). Recombinant protein expression was induced with 1 mM
308 Isopropyl β-D-1-thiogalactopyranoside (*Sigma*; 16°C, 200 RPM, 20 hours). Cells were harvested
309 by centrifugation (5000 RPM, 4°C) and flash frozen in liquid nitrogen.

310 Frozen cell pellets were resuspended in 50 mL of lysis buffer (50 mM Tris-HCl pH 7.5, 300
311 mM NaCl, 30 mM imidazole, 3 mM dithiothreitol, and 1 μM $ZnCl_2$) containing 0.5 mg/mL lysozyme

312 (*Sigma*), 250 U Pierce Universal Nuclease (*ThermoFisher*), and an EDTA-free protease inhibitor
313 cocktail (*Roche*) and rotated at 4°C for 1 hour. The resultant mixture was then sonicated [five
314 cycles of 30 sec on/30 sec off at 50% output] and centrifuged at 4°C, 15,000 RPM for 35 min. The
315 clarified lysate was flowed over a 5 mL HisTrap nickel column (*Cytiva*) using an AKTA Pure FPLC
316 (*Cytiva*) at 0.5 mL/min; all FPLC steps were conducted at 4°C. Unbound molecules were removed
317 with 20 column volumes of wash buffer (WB: 50 mM Tris-HCl, pH 7.5, 300 mM NaCl, 30 mM
318 imidazole, 3 mM DTT, and 1 μM $ZnCl_2$ at 2 mL/min). The 6HIS-tagged MWRA was eluted in a 15-
319 column volume linear gradient from WB to Elution Buffer (WB + 500 mM imidazole) at 2 mL/min.
320 Fractions containing 6HIS-tagged MWRA were identified by SDS-PAGE, pooled, and
321 supplemented with 6HIS-tagged TEV protease (purified as described: Nautiyal and Kuroda, 2018)
322 at a 1:100 enzyme to substrate molar ratio to cleave the 6HIS-tag on WDR5. This mixture was
323 dialyzed against three changes of WB (each 2L for at least four hours at 4°C) and 6HIS-TEV
324 removed from cleaved MWRA via IMAC (Usher et al., 2021). MWRA flow-through protein solution
325 was concentrated to ~15 mL using a 30 kDa MWCO centrifugal filter (*EMD Millipore*), ensuring
326 not to concentrate to where solution became yellow/cloudy and viscous. MWRA complex was
327 resolved over a HiLoad 16/60 Superdex 200 pg gel filtration (GF) column (*Cytiva*) pre-equilibrated
328 in 20 mM Tris-HCl, pH 7.5, 300 mM NaCl, 1 mM TCEP, and 1 μM $ZnCl_2$. Fractions containing
329 stoichiometric MWRA sub-complex were identified by SDS-PAGE, pooled, and concentrated to
330 ~15 mL.

331 HisDPY30 was expressed, purified, and cleaved to remove the 6HIS-tag as described
332 (Patel et al., 2009; Usher et al., 2021). A two-fold molar excess of DPY30 was added to the MWRA
333 sub-complex and incubated on ice for 1 hour. Following incubation, MLL1C was isolated by gel
334 filtration as described for the MWRA complex, with fractions containing the stoichiometric complex
335 identified by SDS-PAGE, pooled, concentrated to ~10 μM, and flash frozen. For dCypher
336 experiments with MLL1C, the 6HIS-tag was retained on DPY30.

337

338 *PTM-defined nucleosomes*

339 All nucleosomes were from the dNuc™ or versaNuc® portfolios (*EpiCypher*). PTMs were
340 confirmed by mass-spectrometry and immunoblotting (if an antibody was available) (Goswami et
341 al., 2021; Marunde et al., 2022b; Weinberg et al., 2019).

342

343 *dCypher assays*

344 *dCypher* binding assays with PTM-defined nucleosomes were performed under standard
345 conditions that titrate query (*e.g.,* epitope-tagged reader domain(s)) to a fixed concentration of
346 target (*e.g.*, biotinylated PTM-defined nucleosome) with the appropriate Alpha Donor and
347 Acceptor beads (*Perkin Elmer*) (Jain et al., 2020; Marunde et al., 2022b; Weinberg et al., 2019).
348 Binding curves [query:target] were generated using a non-linear 4PL curve fit in Prism 9.0
349 (*GraphPad*). For each query, the relative EC_{50} (EC_{50}^{rel}) and hillslope values were derived from the
350 best binding target. EC_{50}^{rel} is the half maximal signal for the specified target. Where necessary,
351 we excluded query concentration values determined to be beyond a query's hook point (signal
352 inhibition due to query exceeding bead saturation). The EC_{80}^{rel} was selected as the optimal
353 probing concentration for discovery screens because of the robust signal-to-background and to
354 provide the best opportunity to bind targets without saturating the primary target signal. To
355 compute EC_{80}^{rel} values, we used the formula $EC_F^{rel} = (F/ (100 – F)^{1/H} \times EC_{50}^{rel}$; F = 80 and H =
356 hillslope.

357 Briefly, 5 µL of GST-tagged reader domain was incubated with 5 µL of 10 nM biotinylated
358 nucleosomes (*e.g., EpiCypher* #16-9001) for 30 minutes at room temperature in 20 mM HEPES
359 pH 7.5, 250 mM NaCl, 0.01% BSA, 0.01% NP-40, 1 mM DTT in a 384-well plate. A mix of 10 uL
360 of 2.5 µg/mL glutathione acceptor beads (*PerkinElmer*, AL109M) and 5 µg/mL streptavidin donor
361 beads (*PerkinElmer*, 6760002) was prepared in 20 mM HEPES pH 7.5, 250 mM NaCl, 0.01%
362 BSA, 0.01% NP-40 and added to each well. The plate was incubated at room temperature in

363 subdued lighting for 60 minutes, and AlphaLISA signal was measured on a PerkinElmer 2104
364 EnVision (680 nm laser excitation, 570 nm emission filter ± 50 nm bandwidth). Each binding
365 interaction was performed in duplicate in a 20 µL mix in 384 well plates.

366 MLL1C binding assays (**Figure 2C**) were performed as described above except using
367 Nickel-chelate acceptor beads (10 µg/mL; *Perkin Elmer* AL108M), streptavidin donor beads (20
368 µg/mL; *Perkin Elmer*) and modified assay buffer (20 mM Tris pH 7.5 + 50 mM NaCl, 0.01% BSA,
369 0.01% NP-40 and 1 mM DTT); [NaCl] was optimized via a titration assay and 50 mM chosen for
370 subsequent analyses.

371

372 In vitro *methylation assays*

373 Methylation assays (Shinsky et al., 2015) were performed at 15°C for three hours using purified
374 MLL1C enzyme and nucleosome substrate in a reaction volume of 20 µL [in 50 mM HEPES, pH
375 8.0, 1 mM DTT, 1 µM $ZnCl_2$; 10 µM of 9:1 *S*-adenosyl-L-methionine (SAM) *p*-toluenesulfonate
376 salt (Sigma) to *S*-adenosyl-L-[*methyl*-^{3}H]-methionine ([*methyl*-^{3}H]-SAM) (*PerkinElmer*)].
377 Concentrations of MLL1C and NaCl were optimized by performing 2D-titration methylation assays
378 at [0, 4 and 40 nM MLL1C] and [0, 50 and 300 mM NaCl] with 2 µg of chicken oligo-nucleosome
379 substrate (Morris et al., 2007). It is notable that, across a range of concentrations, MLL1C stability
380 decreases as temperature increases and methyltransferase activity has been reported to be
381 enhanced in sub-physiological NaCl concentrations (Namitz et al., 2019; Shinsky et al., 2015).
382 For endpoint methylation assays, 4 nM MLL1C and 100 nM nucleosome substrates were tested
383 as above. For steady-state kinetics, 4 nM MLL1C was incubated with a nucleosome substrate
384 titration (0, 23.4, 35.1, 52.7, 79, 119, 178, 267 and 400 nM) and reactions quenched with 5 µL of
385 5X SDS loading dye. For steady-state kinetic assays, 0.5 µg bovine serum albumin was added to
386 each reaction after quenching to act as a loading guide. To analyze methylation, quenched
387 reactions were resolved by 15% Tris-Glycine SDS-PAGE. Gels were stained with Coomassie dye
388 and bands containing mononucleosomes were excised (with serum albumin as a supporting lane

389 marker) and incubated in a solution of 50% Solvable (*PerkinElmer*) and 50% water at 50°C for
390 three hours. Mixture and gel slices were then combined with 10 mL of Hionic-Fluor scintillation
391 fluid (*PerkinElmer*), dark-adapted overnight, and radioactivity measured on a Liquid Scintillation
392 Counter (*Beckman Coulter*).
393
394 *Middle-down mass spectrometry of MCF-7 cells ± KDAC inhibition*
395 MCF-7 breast cancer cells (ATCC HTB-22) were grown in MEM (*Gibco*) supplemented with 10%
396 fetal bovine serum (*VWR*), 100 I.U. penicillin, 100 µg/mL streptomycin (*Corning*), 0.01 mg/mL
397 human recombinant insulin (*Gibco*), and 5 µg/mL plasmocin (*Invivogen*) at 37°C and 5% CO_2.
398 For mass spectrometric (MS) analysis ± KDAC inhibition, cells were cultured in 150 mm
399 dishes to ~80% confluence and treated with 5 mM sodium butyrate (or equivalent volume of water)
400 in triplicate for 0, 10, 20, 30, 60, 120 mins. Cells were washed with cold PBS (11.9 mM
401 phosphates, 137 mM NaCl, 2.7 mM KCl) to remove residual sodium butyrate, harvested by
402 scraping, and flash frozen in liquid nitrogen. Histones were acid extracted after nuclei isolation as
403 described (Holt et al., 2021). Isolated histones were resuspended in 85 µL 5% acetonitrile, 0.2%
404 trifluoroacetic acid (TFA) and resolved by offline high-performance liquid chromatography (HPLC)
405 as described (Holt et al., 2021). Reverse Phase HPLC fractionation was performed with a Thermo
406 U3000 HPLC system (*ThermoFisher*) with a 150 × 2.1–mm Vydac 218TP 3 µm C18 column
407 (*HiChrom* # 218TP3215), at a flowrate of 0.2 mL/min using a linear gradient from 25% B to 60%
408 B in 60 min. The composition of buffers used were A: 5% acetonitrile and 0.2% TFA and B: 95%
409 acetonitrile and 0.188% TFA. After chromatographic separation and fraction collection, histone
410 H3.1 was selected, diluted in 100 mM ammonium acetate (pH = 4) and digested with Glu-C
411 protease (*Roche*) at 10:1 protein:enzyme for 1 h at room temperature prior to mass spectrometric
412 analysis.

413 The digested samples were diluted to 2 µg/µL. Online HPLC was performed on a Thermo
414 U3000 RSLC nano Pro-flow system using a C3 column (Zorbax 300SB-C3, 5 µm; *Agilent*).
415 Samples were maintained at 4 °C and 1 µL injected for each analysis using a microliter pickup. A
416 linear 70-minute gradient of 4-15% B was used (Buffer A: 2% acetonitrile, 0.1% formic acid and
417 Buffer B: 98% acetonitrile and 0.1% formic acid) with a flow rate of 0.2 µL/min. The column eluant
418 was introduced into an Orbitrap Fusion Lumos mass spectrometer (*ThermoFisher*) by nano-
419 electrospray ionization. A static spray voltage of 1900 V and an ion transfer tube temperature of
420 320 °C were set for the source.

421 A Fusion Lumos mass spectrometer was used to generate MS the data. The 9th charge
422 state of histone H3 was targeted for analysis. MS1 analysis was acquired in the orbitrap with a
423 normal mass range and a 60k resolution setting in positive ion mode. An Automatic Gain Control
424 (AGC) target of 5.0E5 with a 200 ms maximum injection time, three microscans, and a scan range
425 of 585-640 *m/z* were used to identify desired ions for fragmentation. MS2 acquisition was
426 performed in both orbitrap and ion trap mode. Both modes used electron transfer dissociation
427 (ETD), a reaction time of 18 ms, and an injection time of 200 ms. A normal scan range was used
428 for the orbitrap mode with a resolution setting of 30k and an AGC target of 5.0E5, with two micro
429 scans. A narrow scan range of 470-530 *m/z*, targeting ions indicative of K4 modification states,
430 was used for the ion trap mode MS2 with an ACG target of 3.0E4, quadrupole isolation, maximum
431 injection time of 100 ms, and eight microscans.

432 These MS methods were used with two technical replicates per biological replicate (n=3).
433 An MS ion trap mode with a targeted mass list was used to increase sensitivity to identify known
434 low abundance K4me3-containing proteoforms. The ion trap MS2 spectra were averaged for each
435 H3 acetyl state based on known retention times, and the intensities of ions indicative of the K4
436 methylation states were manually recorded. Retention times for each acetyl state were
437 approximated as 0ac 35-40 min, 1ac 45-55 min, 2ac 55-60 min, 3ac 62-68 min, 4ac 69-73 min,
438 and 5ac 74-78 min. Precursor mass was used as an additional confirmation and filter of correct

439 acetyl state. For scans yielding low signal and high noise (*i.e.,* 5ac at 0 min butyrate treatment),
440 data were manually curated before averaging. Within acetyl states, the relative proportion of
441 fragment ions for unmodified, mono-, di-, and trimethylation of the H3K4 ion at respective *m/z* of
442 474, 488, 502, and 516 were recorded per MS run. Values were averaged across replicates of
443 the same conditions and normalized to one hundred percent. A two-tailed t-test was used for
444 significance. Raw MS data will be available in a public repository.

445 **REFERENCES**

446 1. Barral, A., Pozo, G., Ducrot, L., Papadopoulos, G.L., Sauzet, S., Oldfield, A.J., Cavalli, G.,
447 and Déjardin, J. (2022). SETDB1/NSD-dependent H3K9me3/H3K36me3 dual
448 heterochromatin maintains gene expression profiles by bookmarking poised enhancers.
449 Molecular Cell *82*, 816-832.e12.
450 2. Garcia, B.A., Pesavento, J.J., Mizzen, C.A., and Kelleher, N.L. (2007). Pervasive
451 combinatorial modification of histone H3 in human cells. Nature Methods *4*, 487–489.
452 3. Ghoneim, M., Fuchs, H.A., and Musselman, C.A. (2021). Histone Tail Conformations: A
453 Fuzzy Affair with DNA. Trends in Biochemical Sciences *46*, 564–578.
454 4. Goswami, J., MacArthur, T., Bailey, K., Spears, G., Kozar, R.A., Auton, M., Dong, J.F.,
455 Key, N.S., Heller, S., Loomis, E., et al. (2021). Neutrophil Extracellular Trap Formation
456 and Syndecan-1 Shedding Are Increased After Trauma. Shock (Augusta, Ga.) *56*, 433–
457 439.
458 5. Greer, E.L., Beese-Sims, S.E., Brookes, E., Spadafora, R., Zhu, Y., Rothbart, S.B.,
459 Aristizábal-Corrales, D., Chen, S., Badeaux, A.I., Jin, Q., et al. (2014). A Histone
460 Methylation Network Regulates Transgenerational Epigenetic Memory in C. elegans. Cell
461 Reports *7*, 113–126.
462 6. Holt, M. v., Wang, T., and Young, N.L. (2019). High-Throughput Quantitative Top-Down
463 Proteomics: Histone H4. Journal of the American Society for Mass Spectrometry *30*,
464 2548–2560.
465 7. Holt, M. v, Wang, T., and Young, N. (2021). Expeditious Extraction of Histones from
466 Limited Cells or Tissue Samples and Quantitative Top-Down Proteomic Analysis. Current
467 Protocols *1*.
468 8. Hörmanseder, E., Simeone, A., Allen, G.E., Bradshaw, C.R., Figlmüller, M., Gurdon, J.,
469 and Jullien, J. (2017). H3K4 Methylation-Dependent Memory of Somatic Cell Identity

470 Inhibits Reprogramming and Development of Nuclear Transfer Embryos. Cell Stem Cell
471 *21*, 135-143.e6.
472 9. Jain, K., Fraser, C.S., Marunde, M.R., Parker, M.M., Sagum, C., Burg, J.M., Hall, N.,
473 Popova, I.K., Rodriguez, K.L., Vaidya, A., et al. (2020). Characterization of the plant
474 homeodomain (PHD) reader family for their histone tail interactions. Epigenetics &
475 Chromatin 2020 13:1 *13*, 1–11.
476 10. Jenuwein, T., and Allis, C.D. (2001). Translating the Histone Code. Science *293*, 1074–
477 1080.
478 11. Lee, Y.T., Ayoub, A., Park, S.H., Sha, L., Xu, J., Mao, F., Zheng, W., Zhang, Y., Cho, U.S.,
479 and Dou, Y. (2021). Mechanism for DPY30 and ASH2L intrinsically disordered regions to
480 modulate the MLL/SET1 activity on chromatin. Nature Communications *12*.
481 12. Marunde, M.R., Fuchs, H.A., Burg, J.M., Popova, I.K., Vaidya, A., Hall, N.W., Meiners,
482 M.J., Watson, R., Howard, S.A., Novitzky, K., et al. (2022a). Nucleosome conformation
483 dictates the histone code. BioRxiv 2022.02.21.481373.
484 13. Marunde, M.R., Popova, I.K., Weinzapfel, E.N., and Keogh, M.-C. (2022b). The dCypher
485 Approach to Interrogate Chromatin Reader Activity Against Posttranslational Modification-
486 Defined Histone Peptides and Nucleosomes. 231–255.
487 14. Mauser, R., Kungulovski, G., Keup, C., Reinhardt, R., and Jeltsch, A. (2017). Application
488 of dual reading domains as novel reagents in chromatin biology reveals a new H3K9me3
489 and H3K36me2/3 bivalent chromatin state. Epigenetics and Chromatin *10*, 1–19.
490 15. Morgan, M.A.J., Popova, I.K., Vaidya, A., Burg, J.M., Marunde, M.R., Rendleman, E.J.,
491 Dumar, Z.J., Watson, R., Meiners, M.J., Howard, S.A., et al. (2021). A trivalent
492 nucleosome interaction by PHIP/BRWD2 is disrupted in neurodevelopmental disorders
493 and cancer. Genes & Development.
494 16. Morris, S.A., Rao, B., Garcia, B.A., Hake, S.B., Diaz, R.L., Shabanowitz, J., Hunt, D.F.,
495 Allis, C.D., Lieb, J.D., and Strahl, B.D. (2007). Identification of histone H3 lysine 36

496 acetylation as a highly conserved histone modification. Journal of Biological Chemistry
497 *282*, 7632–7640.
498 17. Morrison, E.A., Bowerman, S., Sylvers, K.L., Wereszczynski, J., and Musselman, C.A.
499 (2018). The conformation of the histone H3 tail inhibits association of the BPTF PHD finger
500 with the nucleosome. ELife *7*.
501 18. Muramoto, T., Müller, I., Thomas, G., Melvin, A., and Chubb, J.R. (2010). Methylation of
502 H3K4 Is Required for Inheritance of Active Transcriptional States. Current Biology *20*,
503 397–406.
504 19. Musselman, C.A., Lalonde, M.-E., Côté, J., and Kutateladze, T.G. (2012). Perceiving the
505 epigenetic landscape through histone readers. Nature Structural & Molecular Biology
506 2012 19:12 *19*, 1218–1227.
507 20. Namitz, K.E.W., Tan, S., and Cosgrove, M.S. (2019). Hierarchical assembly of the MLL1
508 core complex within a biomolecular condensate regulates H3K4 methylation. BioRxiv
509 870667.
510 21. Nautiyal, K., and Kuroda, Y. (2018). A SEP tag enhances the expression, solubility and
511 yield of recombinant TEV protease without altering its activity. New Biotechnology *42*, 77–
512 84.
513 22. Ng, H.H., Robert, F., Young, R.A., and Struhl, K. (2003). Targeted Recruitment of Set1
514 Histone Methylase by Elongating Pol II Provides a Localized Mark and Memory of Recent
515 Transcriptional Activity. Molecular Cell *11*, 709–719.
516 23. Park, S.H., Ayoub, A., Lee, Y.T., Xu, J., Kim, H., Zheng, W., Zhang, B., Sha, L., An, S.,
517 Zhang, Y., et al. (2019). Cryo-EM structure of the human MLL1 core complex bound to the
518 nucleosome. Nature Communications *10*.
519 24. Patel, A., Dharmarajan, V., Vought, V.E., and Cosgrove, M.S. (2009). On the mechanism
520 of multiple lysine methylation by the human mixed lineage leukemia protein-1 (MLL1) core
521 complex. Journal of Biological Chemistry *284*, 24242–24256.

522 25. Patel, A., Vought, V.E., Dharmarajan, V., and Cosgrove, M.S. (2011). A Novel Non-SET
523 Domain Multi-subunit Methyltransferase Required for Sequential Nucleosomal Histone H3
524 Methylation by the Mixed Lineage Leukemia Protein-1 (MLL1) Core Complex *. Journal of
525 Biological Chemistry *286*, 3359–3369.
526 26. Peach, S.E., Rudomin, E.L., Udeshi, N.D., Carr, S.A., and Jaffe, J.D. (2012). Quantitative
527 Assessment of Chromatin Immunoprecipitation Grade Antibodies Directed against
528 Histone Modifications Reveals Patterns of Co-occurring Marks on Histone Protein
529 Molecules. Molecular & Cellular Proteomics *11*, 128–137.
530 27. Rao, R.C., and Dou, Y. (2015). Hijacked in cancer: The KMT2 (MLL) family of
531 methyltransferases. Nature Reviews Cancer *15*, 334–346.
532 28. Rossetto, D., Avvakumov, N., and Côté, J. (2012). Histone phosphorylation. Epigenetics
533 *7*, 1098–1108.
534 29. Santos-Rosa, H., Schneider, R., Bannister, A.J., Sherriff, J., Bernstein, B.E., Emre, N.C.T.,
535 Schreiber, S.L., Mellor, J., and Kouzarides, T. (2002). Active genes are tri-methylated at
536 K4 of histone H3. Nature 2002 419:6905 *419*, 407–411.
537 30. Sha, L., Ayoub, A., Cho, U.S., and Dou, Y. (2020). Insights on the regulation of the
538 MLL/SET1 family histone methyltransferases. Biochimica et Biophysica Acta - Gene
539 Regulatory Mechanisms *1863*.
540 31. Shinsky, S.A., Monteith, K.E., Viggiano, S., and Cosgrove, M.S. (2015). Biochemical
541 reconstitution and phylogenetic comparison of human SET1 family core complexes
542 involved in histone methylation. Journal of Biological Chemistry *290*, 6361–6375.
543 32. Simon, M.D., and Shokat, K.M. (2012). A Method to Site-Specifically Incorporate Methyl-
544 Lysine Analogues into Recombinant Proteins. Methods in Enzymology *512*, 57–69.
545 33. Smith, L.M., and Kelleher, N.L. (2013). Proteoform: a single term describing protein
546 complexity. Nature Methods 2013 10:3 *10*, 186–187.

547 34. Strahl, B.D., and Allis, C.D. (2000). The language of covalent histone modifications.
548 Nature *403*, 41–45.
549 35. Strahl, B.D., Ohba, R., Cook, R.G., and Allis, C.D. (1999). Methylation of histone H3 at
550 lysine 4 is highly conserved and correlates with transcriptionally active nuclei in
551 Tetrahymena. Proceedings of the National Academy of Sciences *96*, 14967–14972.
552 36. Strelow, J.M., Xiao, M., Cavitt, R.N., Fite, N.C., Margolis, B.J., and Park, K.J. (2016). The
553 Use of Nucleosome Substrates Improves Binding of SAM Analogs to SETD8. Journal of
554 Biomolecular Screening *21*, 786–794.
555 37. Stützer, A., Liokatis, S., Kiesel, A., Schwarzer, D., Sprangers, R., Söding, J., Selenko, P.,
556 and Fischle, W. (2016). Modulations of DNA Contacts by Linker Histones and Post-
557 translational Modifications Determine the Mobility and Modifiability of Nucleosomal H3
558 Tails. Molecular Cell *61*, 247–259.
559 38. Su, Z., and Denu, J.M. (2016). Reading the Combinatorial Histone Language. ACS
560 Chemical Biology *11*, 564–574.
561 39. Tan, S., Kern, R.C., and Selleck, W. (2005). The pST44 polycistronic expression system
562 for producing protein complexes in Escherichia coli. Protein Expression and Purification
563 *40*, 385–395.
564 40. Taverna, S.D., Ueberheide, B.M., Liu, Y., Tackett, A.J., Dias, R.L., Shabanowitz, J., Chait,
565 B.T., Hunt, D.F., and Allis, C.D. (2007). Long-distance combinatorial linkage between
566 methylation and acetylation on histone H3 N termini. Proceedings of the National
567 Academy of Sciences of the United States of America *104*, 2086–2091.
568 41. Taylor, B.C., and Young, N.L. (2021). Combinations of histone post-translational
569 modifications. Biochemical Journal *478*, 511–532.
570 42. Usher, E.T., Namitz, K.E.W., Cosgrove, M.S., and Showalter, S.A. (2021). Probing
571 multiple enzymatic methylation events in real time with NMR spectroscopy. Biophysical
572 Journal *120*, 4710–4721.

43. Vaughan, R.M., Kupai, A., and Rothbart, S.B. (2021). Chromatin Regulation through Ubiquitin and Ubiquitin-like Histone Modifications. Trends in Biochemical Sciences *46*, 258–269.

44. Weinberg, D.N., Papillon-Cavanagh, S., Chen, H., Yue, Y., Chen, X., Rajagopalan, K.N., Horth, C., McGuire, J.T., Xu, X., Nikbakht, H., et al. (2019). The histone mark H3K36me2 recruits DNMT3A and shapes the intergenic DNA methylation landscape. Nature *573*, 281–286.

45. Weinberg, D.N., Rosenbaum, P., Chen, X., Barrows, D., Horth, C., Marunde, M.R., Popova, I.K., Gillespie, Z.B., Keogh, M.C., Lu, C., et al. (2021). Two competing mechanisms of DNMT3A recruitment regulate the dynamics of de novo DNA methylation at PRC1-targeted CpG islands. Nature Genetics *53*, 794–800.

46. Weiss, J.N. (1997). The Hill equation revisited: uses and misuses. The FASEB Journal : Official Publication of the Federation of American Societies for Experimental Biology *11*, 835–841.

47. Wozniak, G., and Strahl, B. (2014). Hitting the “mark”: interpreting lysine methylation in the context of active transcription. Biochimica et Biophysica Acta *1839*, 1353–1361.

48. Xue, H., Yao, T., Cao, M., Zhu, G., Li, Y., Yuan, G., Chen, Y., Lei, M., and Huang, J. (2019). Structural basis of nucleosome recognition and modification by MLL methyltransferases. Nature *573*, 445–449.

49. Young, N.L., DiMaggio, P.A., Plazas-Mayorca, M.D., Baliban, R.C., Floudas, C.A., and Garcia, B.A. (2009). High throughput characterization of combinatorial histone codes. Molecular and Cellular Proteomics *8*, 2266–2284.

50. Young, N.L., DiMaggio, P.A., and Garcia, B.A. (2010). The significance, development and progress of high-throughput combinatorial histone code analysis. Cellular and Molecular Life Sciences 2010 67:23 *67*, 3983–4000.